Machine Learning-Based Cyclostationary Spectrum Sensing in Cognitive Dual Satellite Networks

1st Quynh Tu Ngo
School of Electrical and Data Engineering
University of Technology Sydney
Sydney, Australia
quynhtu.ngo@uts.edu.au

2nd Beeshanga Jayawickrama
School of Electrical and Data Engineering
University of Technology Sydney
Sydney, Australia
beeshanga.jayawickrama@uts.edu.au

3rd Ying He
School of Electrical and Data Engineering
University of Technology Sydney
Sydney, Australia
ying.he@uts.edu.au

4th Eryk Dutkiewicz
School of Electrical and Data Engineering
University of Technology Sydney
Sydney, Australia
eryk.dutkiewicz@uts.edu.au

***Abstract*—Efficient and reliable utilization of the electromagnetic spectrum remains a significant challenge in wireless and satellite communication. To address this, cognitive satellite networks rely on spectrum sensing, a vital aspect that enables the detection and efficient usage of available spectrum. Classic spectrum sensing methods have been developed, with cyclostationary feature detection (CFD) techniques proving robust against noise. However, the adaptation of CFD techniques to cognitive satellite networks is still in its early stages. This paper introduces a machine learning-based cyclostationary spectrum sensing approach for cognitive dual satellite networks, harnessing machine learning to enhance traditional CFD methods in satellite environments. Simulation results demonstrate that the proposed approach surpasses the conventional cyclostationary spectrum sensing method across various signal-to-noise ratio conditions.**

***Index Terms*—Cognitive dual satellite networks, GEO-LEO system, cyclostationary feature detection, machine learning classifiers.**

I. Introduction

Efficient and reliable utilization of the electromagnetic spectrum for communication has been a persistent problem, particularly with the emergence of wireless and satellite technologies. Cognitive satellite networks offer a promising solution to provide reliable and efficient communication services. However, these networks face several challenges, including spectrum scarcity, interference, and signal quality degradation, which can significantly impact their performance. Spectrum sensing, a critical component of cognitive satellite networks, enables the detection of available spectrum and efficient utilization of it. Classic spectrum sensing methods have been developed for this purpose, including energy detection (ED), cyclostationary feature detection (CFD), and matched filter detection (MFD). ED offers low computational complexity and does not necessitate any information regarding the primary user [1], [2], but its decision accuracy is heavily influenced by the accurate noise variance information. CFD performs more stably than ED in the presence of noise uncertainty due to the fact that it is robust to random noise, as noise is usually a stationary signal, while the primary user signal is a cyclostationary signal [3]. MFD is the optimal detection method if the secondary user can obtain prior information about the primary user signal, yet it is challenging to acquire in practice.

This work has been supported by the SmartSat CRC, whose activities are funded by the Australian Government's CRC Program.

Despite the potential benefits of these spectrum sensing techniques, research on adapting them to cognitive satellite networks is still in its infancy. Currently, there are very few studies [4]–[6] on CFD-based spectrum sensing methods for cognitive satellite networks. On the detection of mobile satellite signals, [4] utilized experiments to detect both uplink and downlink signals employing ED and CFD techniques. The findings revealed that while ED exhibits lower computational complexity, it yields lower detection accuracy. On the other hand, CFD, despite being more complex, achieves higher detection accuracy particularly in low SNR scenarios. [5] studied the satellite signal detection blindly through analyzing the signal's cyclic spectrum. The detection method is designed to detect satellite signals in low signal-to-noise ratio (SNR) conditions. However, the proposed method only works effectively when the SNR is above -11 dB. Additionally, [5] did not consider the Doppler effect on satellite signals. [6] considered the impact of the Doppler effect on satellite signals. The study indicated that utilizing a constant Doppler-rate model provides an appropriate signal representation for detecting the presence of cyclostationary narrow-band signals. The detection approach relied on analyzing the cyclic cross-correlation function of signals received at multiple LEO satellites.

In the context of CFD techniques, the classification of signal presence versus noise typically relies on threshold comparison. However, when applying CFD to detect satellite signals, the effectiveness of threshold comparison diminishes, particularly under low SNR conditions. Therefore, in this paper, we propose a machine learning-based cyclostationary spectrum sensing approach for cognitive dual satellite networks (CDSNs). Our approach utilizes the power of machine learning (ML) to enhance the detection performance of traditional CFD methods adopted to satellite networks. ML algorithms are capable of learning complex patterns and relationships in the received signals, enabling them to adaptively adjust the detection threshold based on the cyclostationary characteristics of the received signals. This

adaptability facilitates more accurate discrimination between satellite signals and noise, even in scenarios with low SNR.

The structure of this paper is outlined as follows. Section II elaborates on the CDSN system model, the satellite signal model, and background on the cyclostationary process. The ML-based CFD approach for satellite signals is introduced in Section III, followed by the discussion of simulation results in Section IV. Finally, Section V presents the concluding remarks of the paper.

II. System Model

We consider a CDSN consisting of a GEO satellite S_{GEO}, a LEO satellite S_{LEO}, and a satellite user (SU) on the ground. In this system, S_{LEO} performs spectrum sensing on S_{GEO}'s downlink channel, allowing for opportunistic utilization of the unused spectrum. Let $r(t)$ denote the received signal at S_{LEO}. The spectrum sensing of S_{LEO} at time t can be formulated as a hypothesis testing problem,

$$r(t) = \begin{cases} n(t), & \mathcal{H}_0 \\ y(t) + n(t), & \mathcal{H}_1 \end{cases} \tag{1}$$

where $y(t)$ is the signal received at S_{LEO} transmitted by S_{GEO}, and $n(t) \sim \mathcal{N}(o, \sigma_n^2)$ is the additive white Gaussian noise (AWGN). Here, $\mathcal{H}_0$ and $\mathcal{H}_1$ represent the absence and presence of S_{GEO}'s activity, respectively.

A. Satellite Signal Model

Let a second-order Taylor series approximately represent the propagation delay on $S_{GEO} - S_{LEO}$ link at time t [6] as follows:

$$\mathrm{Z}(t) = \zeta_0 + \zeta_1 t + \zeta_2 t^2, \tag{2a}$$

$$\zeta_0 = \left(\frac{1}{2} a_{GL} t^2 - v_{GL} t + d_0\right)/c, \tag{2b}$$

$$\zeta_1 = (v_{GL} - a_{GL} t)/c, \tag{2c}$$

$$\zeta_2 = a_{GL}/(2c), \tag{2d}$$

where c denotes the speed of light, d_0 represents the initial distance between S_{GEO} and S_{LEO}, v_{GL} and a_{GL} are S_{LEO}'s velocity and acceleration with respect to S_{GEO}, respectively. $v_{GL} = \sqrt{GM/r_L} - \sqrt{GM/r_G}$, where G is the gravitational constant, M is the mass of the Earth, r_L and r_G are the distance from the Earth's center to S_{LEO} and S_{GEO}, respectively. $a_{GL} = -GM/r_L^2 \times e_{r,L} + GM/r_G^2 \times e_{r,G} - 2v_{GL}^2 \times e_{r,G}$ where $e_{r,L}$ and $e_{r,G}$ are the unit vectors in the radical direction from S_{LEO} and S_{GEO} to the Earth's center, respectively.

When S_{GEO} transmits a signal, if the signal bandwidth B and the observation time T_{obs} satisfy the conditions $BT_{obs} \ll |c/v_{GL}|$ and $BT_{obs} \ll |c/a_{GL}|$, then the time stretch in the received signal at S_{LEO} caused by the Doppler effect can be considered negligible [6]. The received signal, under these narrow-band conditions, can be expressed as

$$y(t) = rect(t/T_0) s(t - \zeta_0) e^{-j2\pi f_c(\zeta_1 t + \zeta_2 t^2)}. \tag{3}$$

Here, $s(t)$ represents the signal transmitted by S_{GEO}, and f_c denotes the carrier frequency. The Doppler shift and rate are represented by the terms $-f_c\zeta_1$ and $-2f_c\zeta_2$, respectively. The term $rect(t/T_0)$, where $rect(\cdot)$ denotes the rectangular function, accounts for the time-limited duration of the satellite signal, with a duration of T_0.

B. Background on Cyclostationary Processes

A cyclostationary signal exhibits time-varying statistical properties, unlike stationary signals that remain constant over time. This periodic behavior, resulting from modulation, can be observed in the autocorrelation and spectral density functions. In contrast, noise is typically considered wide-sense stationary with no correlation. Hence, modulated signals and noise can be distinguished by examining the spectral correlation function.

A signal $x(t)$ is classified as cyclostationary if its mean and autocorrelation vary periodically. Its autocorrelation function is denoted as $R_x(t,\tau) = \mathbb{E}\{x(t+\tau/2)x^*(t-\tau/2)\}$. As $R_x(t,\tau)$ exhibits periodicity, it can be expressed as a Fourier series:

$$R_x\left(t - \tau/2, t + \tau/2\right) = \sum_{\alpha} R_x^{\alpha}(\tau) e^{-j2\pi\alpha t} \tag{4}$$

where α and $R_x^{\alpha}(\tau)$ represent the cyclic frequency and the cyclic autocorrelation function (CAC), respectively.

The spectral correlation function (SCF), which represents the cyclic power spectrum of $x(t)$, is derived by taking the Fourier transform of every CAC,

$$S_x^{\alpha}(f) = \int_{-\infty}^{\infty} R_x^{\alpha}(\tau) e^{-j2\pi f\tau} d\tau. \tag{5}$$

The spectral coherence function (SOF), which is the SCF's correlation coefficients, can be computed as

$$C_x^{\alpha}(f) = \frac{S_x^{\alpha}(f)}{\sqrt{S_x^{\alpha}(f - \alpha/2) S_x^{\alpha}(f + \alpha/2)}}. \tag{6}$$

The SOF indicates the strength of the second-order periodicity within the signal. By analyzing the SOF, all statistical characteristics of the signal can be determined.

III. Machine Learning-Based Cyclostationary Feature Detection

The ML-based CFD involves two processes. The first process is the extraction of the cyclostationary features of a detected signal in the form of a cyclic profile. The second process involves using a ML-based classifier to detect S_{GEO}'s spectrum usage based on the cyclic profile of the detected signal.

A. Cyclostationary Feature Extraction for Satellite Signal

Let's consider hypothesis $\mathcal{H}_1$ where $r(t) = y(t) + n(t)$. The autocorrelation function of $r(t)$ can be written as

$$R_r(t,\tau) = R_{yy}(t,\tau) + R_{nn}(t,\tau) + R_{yn}(t,\tau) + R_{ny}(t,\tau) \tag{7}$$

where $R_{yy}(t,\tau)$ and $R_{nn}(t,\tau)$ denote the autocorrelation functions of $y(t)$ and $n(t)$ respectively; $R_{yn}(t,\tau)$ and $R_{ny}(t,\tau)$ are the cross-correlation functions. Since $y(t)$ and $n(t)$ are uncorrelated, we have $R_{yn}(t,\tau) = R_{ny}(t,\tau) = 0$.

The autocorrelation function $R_{yy}(t,\tau)$ can be expressed as

$$\begin{aligned} R_{yy}(t,\tau) =& R_{ss}(t-\zeta_0,\tau)e^{-j2\pi f_c(\zeta_1+2\zeta_2)t}e^{j4\pi f_c\zeta_2 t^2} \\ =& \sum_{\beta} R_{ss}^{\beta}(\tau)e^{j2\pi\beta(t-\zeta_0)}e^{-j2\pi f_c(\zeta_1+2\zeta_2)t}e^{j4\pi f_c\zeta_2 t^2}, \end{aligned} \tag{8}$$

where $R_{ss}(t,\tau)$ denotes the autocorrelation function of $s(t)$, and $R_{ss}^{\beta}(\tau)$ denotes the CAC of $s(t)$ with β represents the cycle frequency exhibited by $s(t)$.

The corresponding CAC can be computed as the coefficients of the Fourier series expression of $R_{yy}(t,\tau)$. Since $y(t)$ is time-limited with T_0 duration, $R_{yy}^{\alpha}(\tau)$ can be expressed as

$$\begin{aligned} R_{yy}^{\alpha}(\tau) =& \frac{1}{T_0}\int_{\frac{-T_0}{2}}^{\frac{T_0}{2}} \sum_{\beta} R_{ss}^{\beta}(\tau)e^{j2\pi\beta(t-\zeta_0)}e^{-j2\pi f_c(\zeta_1+2\zeta_2)t} \\ & \times e^{j4\pi f_c\zeta_2 t^2}e^{-j2\pi\alpha t}dt \\ =& e^{-j2\pi\zeta_0}\sum_{\beta} R_{ss}^{\beta}(\tau) \\ & \times \frac{1}{T_0}\int_{\frac{-T_0}{2}}^{\frac{T_0}{2}} e^{-j2\pi\left(\alpha-\beta+f_c(\zeta_1+2\zeta_2)\right)t}e^{j4\pi f_c\zeta_2 t^2}dt \\ =& \sum_{\beta} R_{ss}^{\beta}(\tau)\mathrm{sinc}\left((\alpha-\beta+f_c(\zeta_1+2\zeta_2)\tau)T_0\right) \\ & \times e^{-j2\pi\zeta_0} \circledast_{\alpha} \mathcal{F}_{\alpha}\left\{rect(t/T_0)e^{-j4\pi f_c\zeta_2 t^2}\right\}, \end{aligned} \tag{9}$$

where $\circledast_{\alpha}$ and $\mathcal{F}_{\alpha}$ denote the convolution and Fourier transform in the cycle frequency domain, respectively.

The corresponding SCF can be expressed as

$$\begin{aligned} S_{yy}^{\alpha}(f) =& e^{-j2\pi\zeta_0}\sum_{\beta} S_{ss}^{\beta}(f) \circledast_f \frac{e^{\frac{-j2\pi f(\alpha-\beta)}{f_c(\zeta_1+2\zeta_2)}}}{f_c(\zeta_1+2\zeta_2)T_0} \\ & \times \left[rect\left(\frac{f-\frac{1}{f_c(\zeta_1+2\zeta_2)T_0}}{\frac{2}{f_c(\zeta_1+2\zeta_2)T_0}}\right)+rect\left(\frac{f+\frac{1}{f_c(\zeta_1+2\zeta_2)T_0}}{\frac{2}{f_c(\zeta_1+2\zeta_2)T_0}}\right)\right] \\ & \circledast_{\alpha,f}\mathcal{F}_{\alpha,f}\left\{rect(t/T_0)e^{-j4\pi f_c\zeta_2 t^2}\right\}, \end{aligned} \tag{10}$$

where $S_{ss}^{\beta}(f)$ denotes the Fourier transform of $R_{ss}^{\beta}(\tau)$.

The CAC and SCF of $n(t)$ are respectively expressed as follows:

$$\begin{aligned} R_{nn}^{\alpha}(\tau) &= \sigma_n^2\delta(\alpha)\delta(\tau), \\ S_{nn}^{\alpha}(f) &= \sigma_n^2\delta(\alpha)\delta(f), \end{aligned} \tag{11}$$

where $\delta(\cdot)$ denotes the Delta function.

We can observe that the AWGN has non-zero SCF values at $\alpha = 0$ and $f = 0$ whereas the received signal $y(t)$ has a non-zero SCF pattern depending on the envelop of $S_{ss}^{\beta}(f)$.

Fig. 1 illustrates the $S_r^{\alpha}(f)$ using the fast spectral correlation estimating method [7] at $SNR = 0dB$ with $s(t)$ is QPSK-modulated, S_{GEO} and S_{LEO} are Inmarsat and Iridium satellites, respectively.

Let's define the cyclic profile of the signal detected at S_{LEO} as $I_r^{\alpha} = \max_f |C_r^{\alpha}(f)|$. By computing the maximum value of the cyclic autocorrelation function over all possible frequencies, the cyclic profile captures the strongest cyclostationary feature in the signal. The cyclic profile is then used as input to the ML-based classifier for S_{GEO}'s spectrum usage detection.

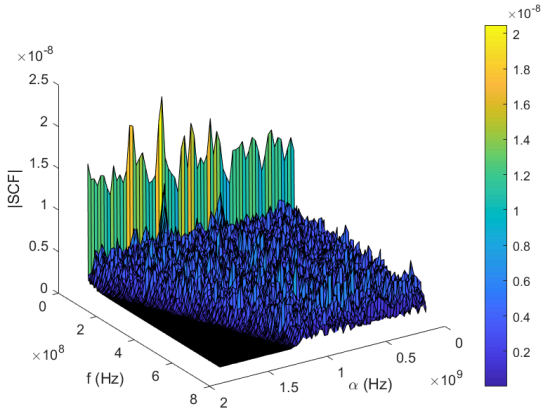

Fig. 1: SCF of a QPSK modulated satellite signal in the presence of noise at $SNR = 0dB$.

B. Machine Learning-Based Classifier

A cyclostationary feature detector computes the weighted estimated SCF by using the ideal SCF as a weighting function. It then compares the weighted estimated SCF to a predefined threshold for signal detection. However, when applied to satellite signals, the detector faces additional challenges. Along with significant fluctuations in signal power due to the long transmission distance, the cyclostationary features of the signal become distorted under Doppler-affected and noisy channel conditions. Consequently, comparing the weighted estimated SCF of a satellite signal to a threshold often leads to false positives, particularly in low SNR scenarios. As a solution, we propose utilizing ML algorithms for detection. Since the detection problem can be framed as a classification problem, we can employ common ML algorithms such as logistic regression (LR), softmax regression (SR), decision tree (DT), and support vector machine (SVM) for signal detection.

1) Logistic Regression: LR is a statistical model that estimates the probability of an event occurring. LR applies a logit transformation to the ratio of the probability of success p to the probability of failure [8]. The logit function is as follows:

$$\begin{cases} \mathrm{Logit}(p) = \frac{1}{1+e^{-p}} \\ \ln\left(\frac{p}{1-p}\right) = W\cdot I_r^{\alpha} \end{cases} \tag{12}$$

where W represents the weight vector, and I_r^{α} is the cyclic profile of the signal. The weight vector W is estimated using maximum likelihood algorithm to optimize the log likelihood function and find the best fit. Once the weight vector is determined, the predicted probability is computed through the conditional probabilities for each observation. For binary classification, probabilities below 0.5 predict 0, while probabilities above 0.5 predict 1.

2) Softmax Regression: While LR is designed for binary classification, SR extends the framework to accommodate multiple class classification. SR assigns probabilities to each class and determines the predicted label by selecting the class with the highest probability. SR employs a separate logit function for each class, calculating the probability of an observation belonging to class k using the softmax function:

$$P(Y = k|X = I_r^\alpha) = \frac{e^{W_k \cdot I_r^\alpha}}{\sum_{i=1}^{K} e^{W_i \cdot I_r^\alpha}}, \tag{13}$$

where W_k denotes the weight vector corresponding to class k with a total of K classes. Training SR follows a similar approach as LR, estimating the weight vectors using a maximum likelihood algorithm to optimize the log-likelihood function.

3) Decision Tree: A DT represents a flowchart-like structure, where each internal node corresponds to a feature or attribute, each branch represents a decision rule based on that attribute, and each leaf node represents the class label. The classification process begins at the root node and proceeds downward through the tree, navigating the appropriate branches based on the input data's feature values. At each internal node, a decision is made based on the selected feature, guiding the path to the next node. This process continues until a leaf node is reached. The predicted label for the input data is determined by the class label associated with the reached leaf node.

4) Support Vector Machine: SVM aims to identify an optimal hyperplane that effectively separates data points belonging to different classes in the feature space. The primary objective of SVM is to maximize the distance between the hyperplane and the nearest data points from each class.

For linearly separable data, SVM constructs a hyperplane defined by

$$W_\perp \cdot I_r^\alpha + b = 0, \tag{14}$$

where $W_\perp$ denotes the weight vector orthogonal to the hyperplane, and b represents the bias term. To address non-linearly separable data, SVM employs a technique known as the kernel trick [8], which transforms the original input space into a higher-dimensional feature space where the data points can be separated by a hyperplane.

Table I illustrates the computational complexity of the aforementioned ML classifiers, including the time complexity and space complexity during both training and testing phases. Here, N denotes the number of training samples, F is the number of features, D refers to the depth of DT, and $\dot{N}$ denotes the number of support vectors in SVM.

TABLE I: Computational complexity

Classifier	Training phase		Testing phase	
	Time	Space	Time	Space
LR	$\mathcal{O}(N \times F)$	$\mathcal{O}(F)$	$\mathcal{O}(F)$	$\mathcal{O}(1)$
SR	$\mathcal{O}(N \times F \times K)$	$\mathcal{O}(F \times K)$	$\mathcal{O}(F \times K)$	$\mathcal{O}(K)$
DT	$\mathcal{O}(N \times \log(N) \times F)$	$\mathcal{O}(D)$	$\mathcal{O}(F)$	$\mathcal{O}(1)$
SVM	$\mathcal{O}(N^2)$	$\mathcal{O}(N \times F)$	$\mathcal{O}(\dot{N} \times F)$	$\mathcal{O}(1)$

IV. Simulation Results

We evaluate the performance of the proposed ML-based CFD algorithms using a dataset of size 3000. This dataset is generated using a cognitive dual satellite network model. In the model, S_{GEO} represents the Inmarsat satellite, and S_{LEO} represents the Iridium satellite. Inmarsat satellite downlink signals are QPSK modulated [9]. The network parameters used to generate the dataset are presented in Table II. The dataset is generated corresponding to the two hypotheses of the testing problem in (1), where for $\mathcal{H}_1$, satellite signals under different SNRs ranging from -30 dB to 0 dB are generated. Next, the entire dataset undergoes cyclic profile computation. Subsequently, the cyclic profile set is randomly partitioned into a training set of size 2400 and a test set of size 600. These sets are employed to train and evaluate the ML classifiers.

TABLE II: Network parameters

Parameter	Description	Value
d_0	$S_{GEO} - S_{LEO}$ initial distance	$35006\ km$
r_G	S_{GEO}-Earth center distance	$42157\ km$
r_L	S_{LEO}-Earth center distance	$7151\ km$
c	speed of light	$3 \times 10^8\ m/s$
G	gravitational constant	$6.674 \times 10^{-11}\ m^3/kg \cdot s^2$
M	Earth mass	$5.972 \times 10^{24}\ kg$
f_c	carrier frequency	$1.530 \times 10^9\ Hz$

TABLE III: Performance report of ML-based cyclostationary spectrum sensing algorithms

	Precision	Recall	F1-score	Support
Logistic Regression				
Chan. idle	0.65	0.80	0.72	260
Chan. busy	0.91	0.79	0.86	340
Accuracy			0.79	600
Macro avg	0.80	0.79	0.79	600
Wt. avg	0.80	0.79	0.79	600
Softmax Regression				
Chan. idle	0.64	0.79	0.71	260
Chan. busy	0.90	0.79	0.85	340
Accuracy			0.79	600
Macro avg	0.80	0.79	0.78	600
Wt. avg	0.80	0.79	0.78	600
Decision Tree				
Chan. idle	0.68	0.68	0.68	260
Chan. busy	0.68	0.68	0.68	340
Accuracy			0.68	600
Macro avg	0.68	0.68	0.68	600
Wt. avg	0.68	0.68	0.68	600
Support Vector Machine				
Chan. idle	0.63	0.9	0.74	260
Chan. busy	0.92	0.76	0.84	340
Accuracy			0.79	600
Macro avg	0.83	0.75	0.79	600
Wt. avg	0.83	0.75	0.79	600

The performance evaluation of the proposed algorithms is presented in Table III, showcasing precision, recall, F1-score, and prediction accuracy. Precision determines the ratio of correctly predicted positive instances among all positive predictions. Recall assesses the ratio of correctly predicted positive instances among all actual positive samples in the

test set. The F1-score represents the harmonic mean of precision and recall. Additionally, the support column indicates the number of data samples for each class.

We observe that LR, SR, and SVM achieved similar detection accuracy of 79.36%, 79.39%, and 79.48%, respectively, while DT only achieved an accuracy of 68.27%. LR and SR exhibited identical performance in terms of precision, recall, F1-score, and accuracy. SVM had the highest precision for class 1 (channel busy class), with a score of 0.92, but a lower recall score of 0.76 compared to LR and SR. This implies that SVM correctly identified a high proportion of actual positive samples but also misclassified some positive samples as negative, leading to a lower F1-score for class 1.

The simulation results presented in Fig. 2 evaluate the prediction accuracy under various SNRs. The comparison is made between the CFD method with threshold comparison [10] and the proposed ML-based methods. In the CFD-threshold method, the determination of threshold values relies on the statistical characteristics of the cyclic profile of the received satellite signals [10]. This method serves as a benchmark for evaluating the performance of the ML-based approaches.

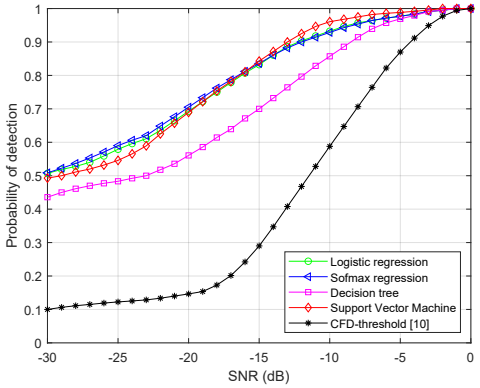

Fig. 2: Detection accuracy of different ML-based cyclostationary spectrum sensing algorithms.

To assess the effectiveness of the ML-based methods, Receiver Operating Characteristic (ROC) curves are employed, specifically at an SNR of -10 dB, as depicted in Fig. 3. The ROC curves visualize the trade-off between detection accuracy and false alarm rates. The results reveal that the ML-based methods surpass the conventional CFD method in terms of performance. Even in extremely low SNR regions (below -15 dB), the ML-based methods demonstrate the ability to detect spectrum usage accurately. These findings are consistent with the observations presented in Table III, where the LR and SVM models exhibit nearly identical performance. However, in SNR regions lower than -16 dB, SVM outperforms LR and demonstrates superior classification capability. Additionally, the DT algorithm consistently exhibits the poorest performance among the ML-based methods. Considering the trade-off between computational resources and accuracy requirements, both LR and SVM are viable classifiers to consider based on the specific demands of the application at hand.

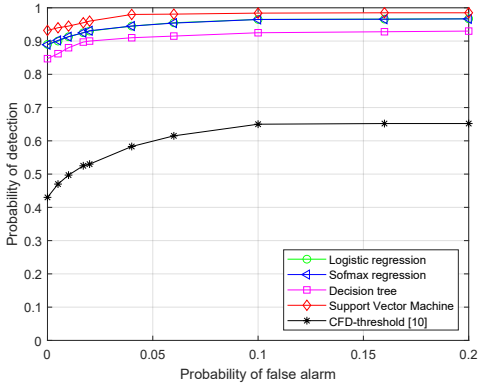

Fig. 3: ROC curves of different ML-based cyclostationary spectrum sensing algorithms at SNR = -10 dB.

V. Conclusions

In this paper, we presented a ML-based approach for cyclostationary spectrum sensing in CDSN. Our proposed approach demonstrated effective performance in low SNR conditions and outperformed the conventional cyclostationary spectrum sensing method. LR, SR, DT, and SVM were employed as classifiers in the proposed approach, yielding detection accuracies of 79.36%, 79.39%, 68.27%, and 79.48%, respectively. Simulation results under a wide range of low SNRs further confirmed the effectiveness of our proposed ML-based approach.

References

[1] B. A. Jayawickrama, E. Dutkiewicz, M. Mueck, and Y. He, "On the usage of geolocation-aware spectrum measurements for incumbent location and transmit power detection," *IEEE Trans. Veh. Technol.*, vol. 65, no. 10, pp. 8177–8189, 2016.

[2] S. Basnet, Y. He, E. Dutkiewicz, and B. A. Jayawickrama, "Resource allocation in moving and fixed general authorized access users in spectrum access system," *IEEE Access*, vol. 7, pp. 107 863–107 873, 2019.

[3] M. Mueck, Y. He, B. Jayawickrama, and E. Dutkiewicz, "Methods and devices for user detection in spectrum sharing," Patent US10 681 558B2, Jun 09, 2020. [Online]. Available: https://patents.google.com/patent/US10681558B2/en.

[4] F. Dimc, G. Baldini, and S. Kandeepan, "Experimental detection of mobile satellite transmissions with cyclostationary features," *Int. J. Satell. Commun. Network.*, vol. 2, no. 1, pp. 100–121, 2014.

[5] Q. Wang, Z. Xie, J. Hu, and G. Zhang, "Blind detection of satellite communication signals based on cyclic spectrum," in *2015 Int. Conf. Wirel. Commun. Signal Process. (WCSP)*, 2015, pp. 1–5.

[6] J. Hofmann, T. Delamotte, and A. Knopp, "Cyclostationarity-based signal detection in multi-satellite systems: Invited paper," in *2022 56th Asilomar Conf. Signal Syst. Comput.*, 2022, pp. 877–880.

[7] J. Antoni, G. Xin, and N. Hamzaoui, "Fast computation of the spectral correlation," *Mech. Syst. Signal Process.*, vol. 92, pp. 248–277, 2017.

[8] G. Bonaccorso, *Machine learning algorithms*. Packt Publishing, 2017.

[9] J. Boseman, "Feasibility of a dynamic data rate satellite link for inmarsat," Master Thesis, Naval Postgraduate School, Monterey, CA, US, 2007.

[10] B. Kumar, V. Bindu, and N. Swetha, "User detection using cyclostationary feature detection in cognitive radio networks with various detection criteria," in *Int. Conf. Innov. Comput. Commun.*, 2021, pp. 1013–1029.